FULL PAPER

The LEGATOS technique: A new tissue-validated dynamic contrast-enhanced MRI method for whole-brain, high-spatial resolution parametric mapping

Ka-Loh Li[1] (ID) | Daniel Lewis[1,2,3] | David J. Coope[2,3,4] | Federico Roncaroli[3,4] | Erjon Agushi[1] | Omar N. Pathmanaban[2,3,5] | Andrew T. King[2,3,6] | Sha Zhao[1] | Alan Jackson[1] | Timothy Cootes[1] | Xiaoping Zhu[1]

[1]Division of Informatics, Imaging and Data Sciences, University of Manchester, Manchester, United Kingdom

[2]Department of Neurosurgery, Manchester Centre for Clinical Neurosciences, Salford Royal NHS Foundation Trust, Manchester Academic Health Science Centre, Manchester, United Kingdom

[3]Geoffrey Jefferson Brain Research Centre, University of Manchester, Manchester, United Kingdom

[4]Division of Neuroscience and Experimental Psychology, School of Biological Sciences, Faculty of Biology, Medicine and Health, University of Manchester, Manchester, United Kingdom

[5]Division of Cell Matrix Biology & Regenerative Medicine, School of Biological Sciences, Faculty of Biology Medicine and Health, University of Manchester, Manchester, United Kingdom

[6]Division of Cardiovascular Sciences, School of Medical Sciences, Faculty of Biology Medicine and Health, University of Manchester, Manchester, United Kingdom

Correspondence
Ka-loh Li, Wolfson Molecular Imaging Centre, University of Manchester, 27 Palatine Road, Manchester M20 3LJ, United Kingdom.
Email: ka-loh.li-2@manchester.ac.uk

Funding information
Cancer Research UK (CRUK) and the Engineering and Physical Sciences Research council (ESPRC) through the Cancer Imaging Centres grant, Grant/Award Number: C8742/A18097; Dowager Countess Eleanor Peel Trust

Purpose: A DCE-MRI technique that can provide both high spatiotemporal resolution and whole-brain coverage for quantitative microvascular analysis is highly desirable but currently challenging to achieve. In this study, we sought to develop and validate a novel dual-temporal resolution (DTR) DCE-MRI-based methodology for deriving accurate, whole-brain high-spatial resolution microvascular parameters.

Methods: Dual injection DTR DCE-MRI was performed and composite high-temporal and high-spatial resolution tissue gadolinium-based-contrast agent (GBCA) concentration curves were constructed. The high-temporal but low-spatial resolution first-pass GBCA concentration curves were then reconstructed pixel-by-pixel to higher spatial resolution using a process we call LEGATOS. The accuracy of kinetic parameters (K^{trans}, v_p, and v_e) derived using LEGATOS was evaluated through simulations and in vivo studies in 17 patients with vestibular schwannoma (VS) and 13 patients with glioblastoma (GBM). Tissue from 15 tumors (VS) was examined with markers for microvessels (CD31) and cell density (hematoxylin and eosin [H&E]).

Results: LEGATOS derived parameter maps offered superior spatial resolution and improved parameter accuracy compared to the use of high-temporal resolution data alone, provided superior discrimination of plasma volume and vascular leakage

Ka-Loh Li and Daniel Lewis contributed equally to this work.

effects compared to other high-spatial resolution approaches, and correlated with tissue markers of vascularity ($P \leq 0.003$) and cell density ($P \leq 0.006$).

Conclusion: The LEGATOS method can be used to generate accurate, high-spatial resolution microvascular parameter estimates from DCE-MRI.

1 | INTRODUCTION

Kinetic parameters derived from DCE-MRI are increasingly used in the study of tumors, both within and outside the brain, for assessment of tumor microenvironment and microvasculature. They have demonstrable value as predictive, prognostic, and treatment response biomarkers and are of increasing importance with the growing use of anti-angiogenic therapies.[1-7] Key limitations in current DCE-MRI techniques include the volume coverage, spatial resolution and accuracy of derived kinetic parameters, and the requirement for full-dose gadolinium-based-contrast agent (GBCA) administration during data acquisition.[8-13] Whereas whole-brain coverage and high-spatial (HS) resolution are essential where lesions are widespread, small, or exhibit significant microvascular heterogeneity, high-temporal (HT) resolution is required for accurate quantification of kinetic parameters such as cerebral blood flow, fractional plasma volume (v_p), transfer constant (K^{trans}), and the fractional volume of extravascular extracellular space (v_e).[14-16]

Traditional Cartesian MRI has limitations in achieving simultaneous HS and HT resolution so that a compromise must be made in the protocol design. Dual-temporal resolution (DTR) techniques incorporating a staged dual-bolus of GBCA have been developed to address this limitation.[17] Li and colleagues measured plasma concentration curves from an initial low-dose high-temporal (LDHT) resolution acquisition to reconstruct a HT resolution vascular input function (VIF).[18] This accurate VIF was then used for subsequent kinetic analysis of a second full-dose HS resolution (FDHS) data set. This approach, termed the dual injection contrast enhanced (DICE)-FDHS method, generated HS resolution parametric maps, however, the low-temporal resolution (frame duration $\Delta t = 10$ s) of the GBCA uptake curves in tissue resulted in covariate errors during kinetic fitting, observable as large vessel and vascular leakage contamination within the derived K^{trans} and v_p maps, respectively.[17]

DTR DCE-MRI methods that can provide accurate pharmacokinetic estimates with high spatiotemporal resolution are, therefore, needed. Both dual injection and a single low-dose injection DTR DCE-MRI have shown the potential to provide high spatiotemporal resolution and whole-brain coverage for quantitative microvascular analysis.[19-21] This paper focuses on the dual injection technique. The aims of this feasibility study are therefore (1) to develop a new analysis technique, the level and rescale the gadolinium contrast concentration curves of high-temporal to high-spatial (LEGATOS) method, for deriving accurate, whole-brain high-spatial resolution microvascular parameters from dual injection DTR DCE-MRI data, and (2) to validate parameter estimates derived using the LEGATOS method using both computer simulation and an in vivo study incorporating correlation with histopathological data.

2 | METHODS

2.1 | Patients

For this feasibility study, we investigated previously acquired dual injection DTR DCE-MRI data in 13 patients with glioblastoma (GBM) and 17 patients with vestibular schwannoma (VS) (including 1 patient with bilateral neurofibromatosis type 2 [NF2]-related VS). Although GBM are the most common malignant brain tumor in adults, VS were also chosen as a disease model because they are not influenced by brain microenvironment and its vasculature because of their extra-axial location. In addition, smaller tumors can be resected whole permitting more robust comparisons between imaging and tissue data. The study obtained ethical approval (NHS Health Research Authority; NRES committee North West 13/NW/0131 and 13/NW/0247), and all participants provided informed consent.

2.2 | MR imaging

Imaging was performed on 2 Philips Achieva whole body scanners (Philips, Best, Netherlands) with most patients scanned at 1.5T (1 patient with a sporadic VS was scanned at 3.0T). For all studie, a macrocyclic GBCA (gadoterate meglumine; Dotarem, Guerbet S.A.) was administered by power injector as an intravenous bolus at a rate of 3 mL/s, followed by a chaser of 20 mL of 0.9% saline administered at the same

rate. High-resolution 3D T_1-weighted (T_1W) gradient echo sequence with whole-brain coverage (TE = 3.2 ms, TR = 8.6 ms, slice thickness = 1.2 mm) both before and after contrast were obtained for tumor delineation.

Data were acquired using a previously described DTR, DICE technique.[17] For the first part of this DTR technique, a low-dose fixed-volume of GBCA was administered during acquisition of a HT resolution sequence using a 3D gradient echo sequence with a flip angle of 20°, TR/TE of 2.5 ms/0.696 ms, SENSE acceleration factor of 1.8, reconstructed matrix size of 96 × 96 × 22, voxel size of 2.5 × 2.5 × 6.35 mm³, pixel bandwidth of 700 Hz, and frame duration (Δt) of 1.0 s ($n = 300$). This was followed by a full-dose of GBCA (dose = 0.2 mL/kg × weight − dose of prebolus) administered during acquisition of a HS resolution sequence with a flip angle of 20°, TR/TE of 3.7 ms/0.93 ms, SENSE acceleration factor of 2.8, reconstructed matrix size of 240 × 240 × 70, reconstructed voxel size of 1 × 1 × 2 mm³, pixel bandwidth of 700 Hz, and frame duration (Δt) of 10.7 s ($n = 60$). For both the LDHT and FDHS acquisition, 0 padding was used for FFT reconstruction in the z-direction, which doubles the number of slices. For baseline longitudinal relaxation rate ($R1_0$) mapping, variable flip-angle (VFA; $\alpha = 2°, 8°, 15°$, and 20°) acquisitions were undertaken before both the LDHT and FDHS DCE series. The spatial resolution of each VFA acquisition series was chosen to match the LDHT (2.5 × 2.5 × 6.35 mm³) and FDHS (1 × 1 × 2 mm³) DCE series, respectively.

2.3 | The new DTR DCE-MRI processing method

Our new DTR-based mapping technique relied on 2 key steps, which can be summarized as follows:

> Key step I: combination of the HT and HS resolution series to construct a 4D GBCA concentration volume (HTHS-merged) with a HT arterial phase followed by a HS parenchymal tissue phase.

A 2-part 4D GBCA concentration volume, termed HTHS-merged, was constructed from the HT (high-temporal, low-spatial) and HS (high-spatial, low-temporal) resolution dynamic series. The native 4D HT dynamic images (voxel size = 2.5 × 2.5 × 6.35 mm³) were first co-registered and resliced to a HS baseline image frame (voxel size = 1 × 1 × 2 mm³) using a 4th degree B-spline interpolation within statistical parametric mapping[22] to obtain a 4D $HT_{aligned}$ volume (voxel size = 1 × 1 × 2 mm³). The signal intensity-time curves from this 4D $HT_{aligned}$ and the 4D HS dynamic image volumes were then converted to GBCA concentration-time curves using their respective baselines and $R1_0$ derived from the pre-injection VFA acquisitions.

The constructed DTR 4D GBCA concentration volume (HTHS-merged) must retain an HT arterial phase to enable accurate discrimination between plasma volume and vascular leakage effects. The initial 40 s of the $HT_{aligned}$ concentration-time course was, therefore, concatenated with later concentration-time points obtained from the FDHS series. The time point for this adjoining (t_{adj}) was selected to be just after the recirculation phase to limit the effects of rapid systemic contrast agent leakage and fluctuations because of recirculation. Because of the differences in administered dose and time of GBCA administration between the LDHT and FDHS DCE series, the later phase of the HS concentration curves also needed to be cross-calibrated with the HT curves for both bolus arrival time (BAT) and GBCA dose before concatenation.[19]

The major steps in the construction of the DTR 4D concentration volume from the dual injection DTR data are illustrated in Figure 1.

> Key step II: pixel-by-pixel rescaling the concatenated HT arterial phase to resemble the supposed "true" HS resolution arterial phase using LEGATOS.

Through containing an initial HT arterial phase ($HT_{aligned}$) followed by a HS parenchymal tissue phase, the HTHS-merged volume maintains the temporal fidelity of the arterial phase of the LDHT series. Despite the HT data set being resampled/interpolated in image space to higher spatial resolution, however, the observed $HT_{aligned}$ data (voxel size = 1 × 1 × 2 mm³) still primarily reflects the arterial phase of the acquired low-spatial resolution pixel GBCA concentration curve and must be replaced with a reconstructed HS arterial phase. Without this reconstruction step parameter maps (in particular v_p) derived from kinetic fitting of the 4D HTHS-merged concentration volume generated in key step I would still closely resemble those obtained from the native low-spatial resolution LDHT DCE data set.

In key step II, LEGATOS was therefore used for pixel-by-pixel reconstruction of the concatenated low-spatial resolution HT arterial phase of the HTHS-merged concentration volume to reflect the supposed "true" HS resolution one. This pixel-wise reconstruction method was based on the fact that the GBCA concentration value is not affected by the imaging parameters. Rather, the observed difference in the GBCA concentration between the concatenated $HT_{aligned}$ and dose-adjusted HS concentration curves in each pixel of the HTHS-merged 4D concentration volume (Figure 2, left column, voxel size = 1 × 1 × 2 mm³) reflects the difference in the native spatial resolution during data acquisition and any possible effects of the statistical parametric mapping interpolation of the native HT arterial phase; assuming there is no dominant noise process affecting estimated GBCA concentration. In addition,
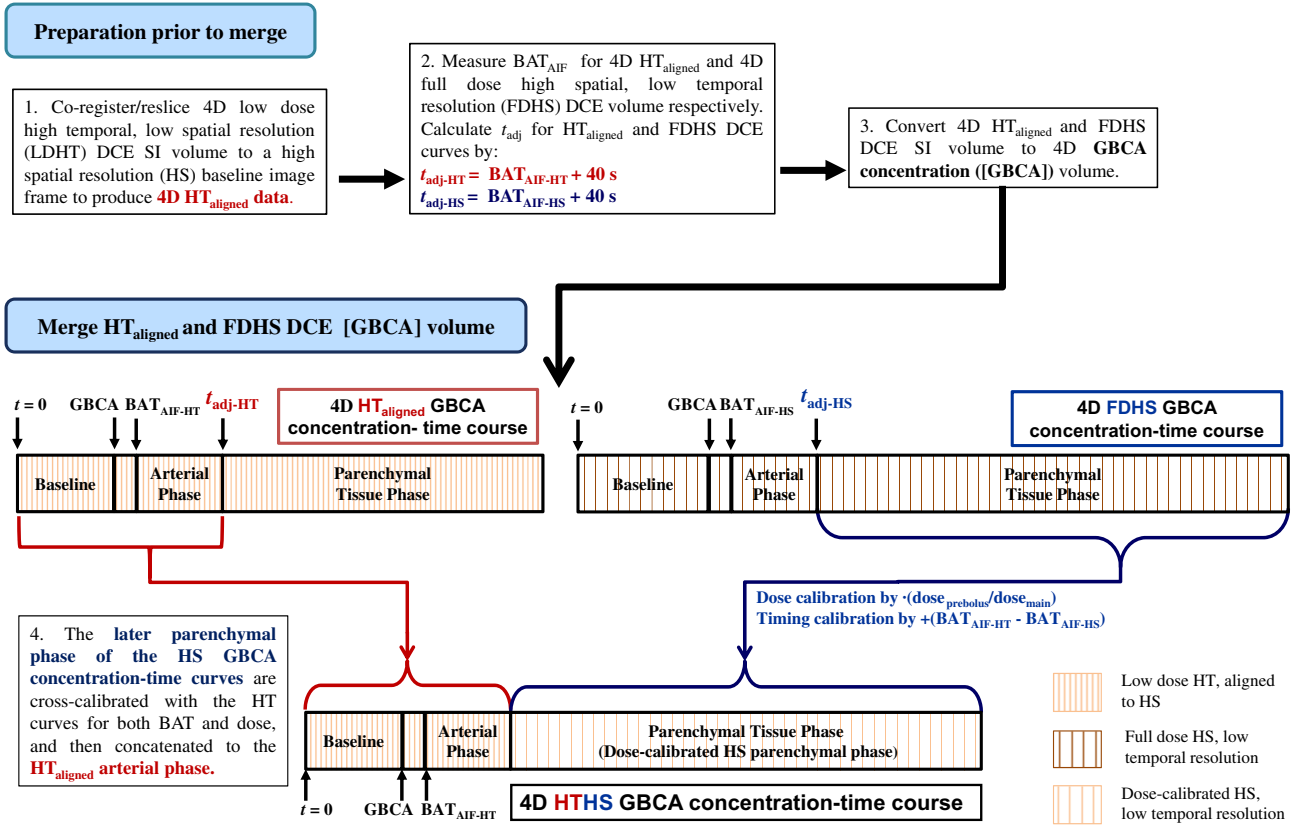
FIGURE 1 Combination of the low-dose high-temporal (LDHT) and full-dose high-spatial (FDHS) data from dual injection DTR MRI. Combination of the low-dose high-temporal (LDHT) and full-dose high-spatial (FDHS) GBCA concentration-time curves from dual injection dual-temporal resolution DCE MRI data are shown. The LDHT data are first co-registered to a HS baseline image frame and interpolated to generate a 4D $HT_{aligned}$ DCE data set with the same x, y, and z dimensions ($1 \times 1 \times 2$ mm^3) as each HS image frame. To allow for timing cross-calibration in the subsequent merge process, the arterial input function bolus arrival time (BAT_{AIF}) and the time point for adjoining the $HT_{aligned}$ and FDHS concentration-time curves (t_{adj}) are derived for the LDHT and FDHS data sets, respectively. The 4D $HT_{aligned}$ and FDHS signal intensity (SI) DCE volumes are then converted to 4D GBCA concentration volumes. For the merge process the later parenchymal phase of the FDHS concentration-time curves are cross-calibrated with the LDHT curves for both timing and GBCA dose and are then concatenated to the arterial phase of the low-dose $HT_{aligned}$ data set to generate a HTHS-merged 4D concentration volume. GBCA = gadolinium-based-contrast agent

the LEGATOS method assumes that in each tissue pixel of the HTHS-merged 4D concentration volume generated in key step I, the supposed "true" HS resolution arterial phase has the same shape as the observed $HT_{aligned}$ arterial phase, so it can be obtained by re-scaling the $HT_{aligned}$ arterial phase using a calibration ratio, $ratio_{calib}$. Therefore,

$$C_{t-HS}(t) = C_{t-HT}(t) \cdot ratio_{calib}, \quad t \leq t_{adj}, \quad (1)$$

where $C_{t-HT}(t)$ is the observed $HT_{aligned}$ arterial phase concentration-time curve, $C_{t-HS}(t)$ is the supposed "true" HS arterial phase concentration-time curve, and

$$ratio_{calib} = C_{t-HS}(t_{adj}) / C_{t-HT}(t_{adj}). \quad (2)$$

The calibration ratio was calculated from the concatenated HTHS-merged concentration-time curve by taking the ratio of the mean concentration of 5 HS frames following the concatenation time point, t_{adj}, over the mean concentration of 4 final frames of the $HT_{aligned}$ arterial phase series before t_{adj}. This calibration ratio was then used to rescale the

initial $HT_{aligned}$ arterial phase of each pixel concentration-time curve to achieve a smooth concatenation with the later HS parenchymal phase before kinetic fitting (Figure 2). The LEGATOS method will automatically adjust this calibration ratio and scaling procedure to achieve a smooth concatenation between the $HT_{aligned}$ and HS concentration-time curves. As such, although the first-pass bolus shape of the $HT_{aligned}$ curve is propagated through to the reconstructed arterial phase of the HS curve, any scale change (eg, because of statistical parametric mapping interpolation) of the $HT_{aligned}$ arterial phase will not be propagated through to the final concentration-time curve.

2.4 | Kinetic analysis

The extended Tofts model (ETM) was fitted to the tissue GBCA concentration-time curves of the 4D HTHS-merged concentration volume from each patient.[23,24] This fitting was
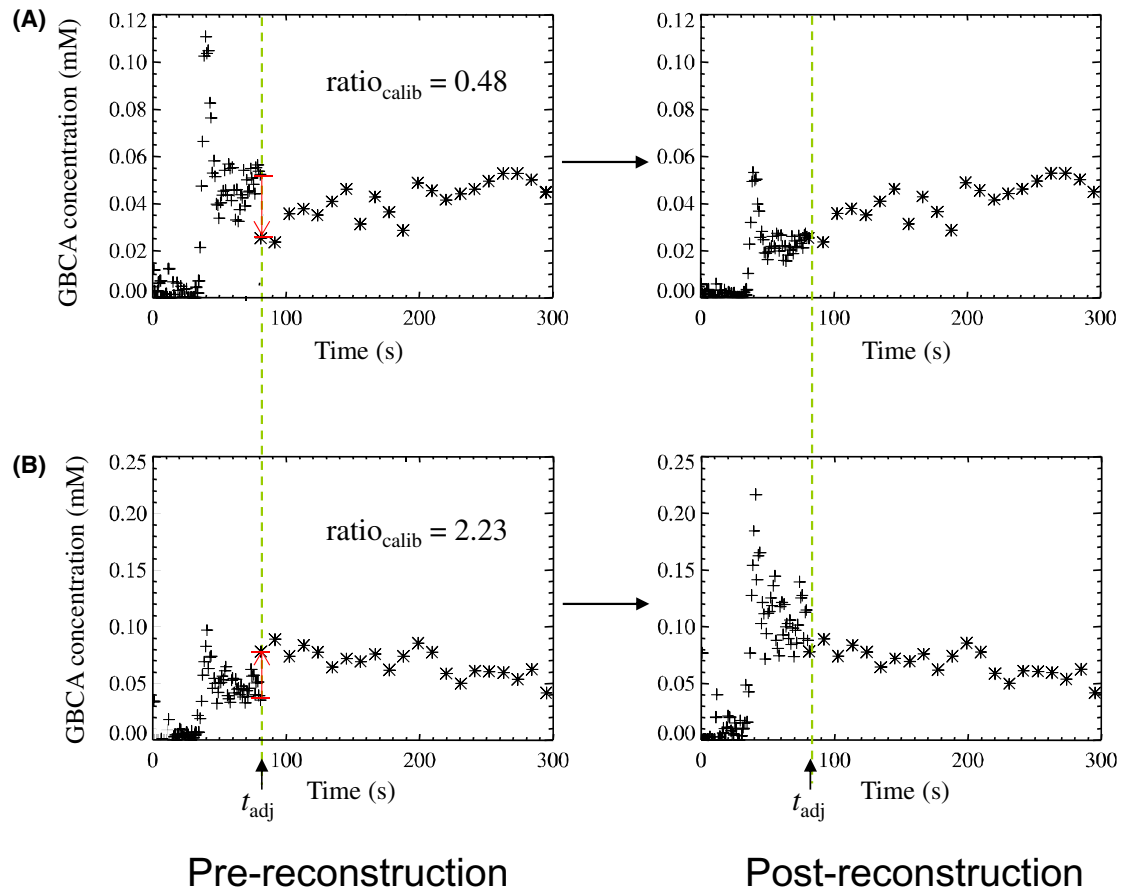
FIGURE 2 Pixel-by-pixel rescaling of the HT arterial-phase of the HTHS-merged concentration-time curve to resemble the supposed "true" high-spatial resolution one. Panels (A) and (B) show 2 representative pixels from the tissue GBCA concentration-time curve in a VS imaged at 3T. The left column represents the HTHS-merged concentration-time curve in each pixel and the right column shows the rescaling of the HT arterial-phase to achieve a smooth concatenation with the later parenchymal HS phase. Ratio$_{calib}$ is used to rescale the initial $C_{t\text{-}HT}(t)$ for each pixel, so that the $C_{t\text{-}HT}(t)$ and $C_{t\text{-}HS}(t)$ are concatenated, although maintaining the shape of the first-pass $C_{t\text{-}HT}(t)$ curve. $C_{t\text{-}HT}(t)$ is the HT$_{aligned}$ arterial phase GBCA concentration-time curve; $C_{t\text{-}HS}(t)$ is the parenchymal HS GBCA concentration-time curve; ratio$_{calib}$ = ratio of the mean concentration of several HS frames following the time point for the concatenation (t_{adj}) over the mean concentration of several ending frames of the HT arterial phase series

performed either immediately following key step I (HTHS-merged method), or following both key steps I and II above (the LEGATOS method). In both cases the final spatial resolution of derived kinetic parameter maps was $1 \times 1 \times 2$ mm. Kinetic analysis was also performed using the LDHT or FDHS tissue GBCA concentration-time curves alone as a comparative measure. The dynamic MR signal measured from voxels in the vertical part of superior sagittal sinus was used as an indirect estimate of the arterial input function as described previously[25,26] (Supporting information Figure S1). As part of the fitting procedure the BAT for each tissue voxel is estimated and the $C_p(t)$ measured from the superior sagittal sinus time-shifted to align with the BAT of each tissue GBCA concentration-time curve. A map of scaled fitting error (SFE)[27] was generated as an integral part of each fitting procedure to assess the discrepancy between the derived curve and the original data and tumor voxels with an SFE value above 50% were excluded from the statistics. In all cases to confirm the acceptance of the use of SFE > 50% for

excluding outlier tumor voxels, visual inspection of derived SFE and kinetic parameter maps (before and after exclusion of voxels with SFE > 50%) was performed.

2.5 | Computer simulation to evaluate the LEGATOS method

Dual injection DTR MRI data obtained from a patient with a sporadic VS imaged at 3T was used as the base for the computer simulation.[20] HS resolution parameter estimates for K^{trans}, v_p, v_e, and bolus arrival time (t0), derived from the LEGATOS analysis were used as the "true" values for simulation of a 4D FDHS GBCA concentration volume. The combined low-dose $C_p(t)$ curve used as a VIF for the in vivo LEGATOS analysis (Figure 3A) was time-shifted and summed to generate a full-dose, HT resolution VIF for use in the simulation of tissue enhancement curves (Figure 3B). The simulated tissue voxel concentration-time curves were then
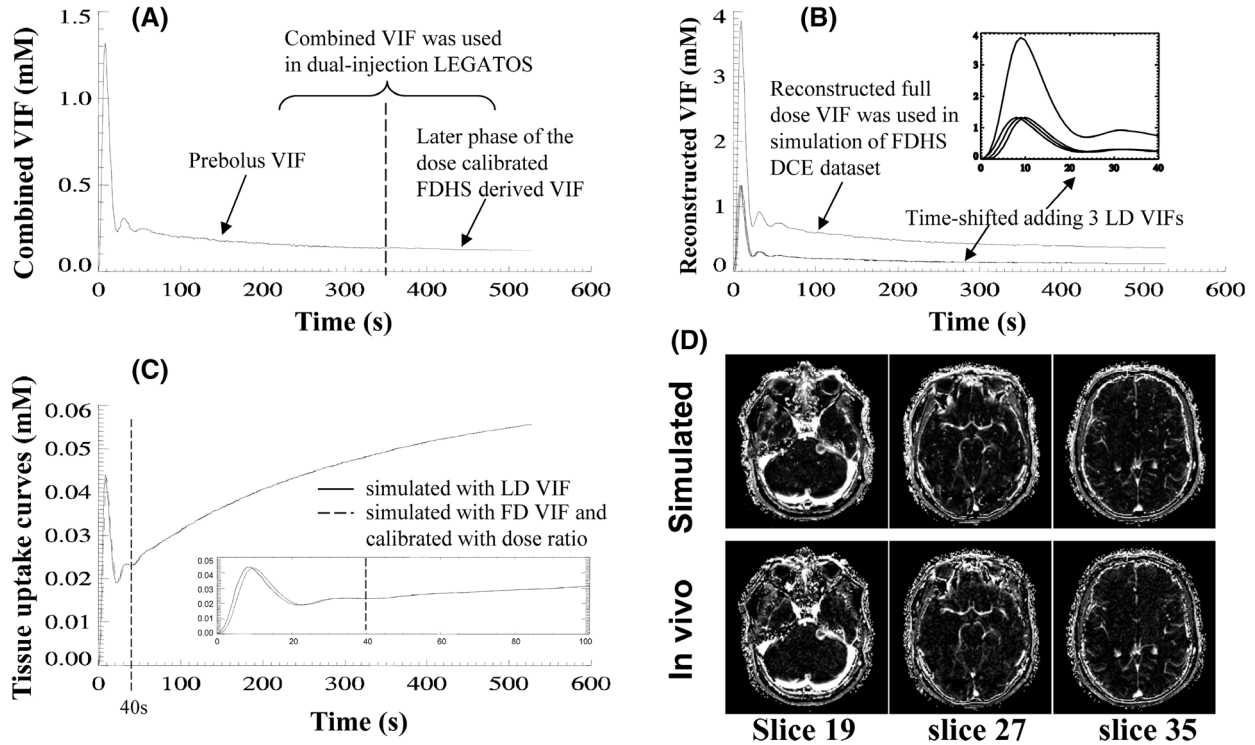
FIGURE 3 Computer simulations to evaluate the LEGATOS method. Panels (A)-(D) demonstrate simulation of dual injection DCE (DICE) data. (A) Combined low-dose (LD) vascular input function (VIF) used for the in vivo LEGATOS analysis. The VIF shown was derived from a 71-year-old patient with a left-sided, sporadic VS who underwent dual injection (3 mL and 9.4 mL of GBCA, respectively), DTR DCE MRI at 3T. (B) Reconstructed VIF used for the full-dose high-spatial resolution (FDHS) DCE data simulation. This VIF was derived by time-shifting and adding 3 of the low-dose VIFs shown in panel A (The small panel with a time window of 40 s in the upper-right corner of the graph demonstrates more details of the time-shifted VIF addition). (C) Tissue uptake curves simulated using either the in vivo low-dose VIF shown in panel A (solid curve) or simulated using the reconstructed full-dose VIF show in panel B and rescaled with the dose ratio (dashed curve). Concentration-time curves were simulated using $K^{trans} = 0.03$ min^{-1}, $v_e = 0.6$, and $v_p = 0.03$. The small panel with a time window of 100 s gives more details of the comparison. (D) Three representative slices from a time frame ($t = 40$ s) of the simulated 4D FDHS DCE images (top row), compared with matched imaging from the in vivo 4D FDHS data (bottom row)

resampled with a temporal interval of 10-s to resemble the in vivo acquired FDHS-DCE data set.

Quantitative image comparisons between the in vivo acquired and the simulated 4D FDHS concentration volumes were performed using the structural similarity index.[28] The mean structural similarity index values between 2 images were calculated using the same slice level within the 2 volumes. The simulated FDHS-DCE data set was then combined with the in vivo LDHT data set to construct a HTHS-merged 4D concentration volume as described in key step I. The ETM was then either directly fitted to the tissue GBCA concentration-time curves of this 4D HTHS-merged concentration volume (HTHS-merged method), or undertaken following initial HT concentration-time curve rescaling (the LEGATOS method), yielding "measured" K^{trans}, v_p, v_e, and t0 maps.

2.6 | Tissue analysis

Tissues from 15 sporadic VS were analyzed. Ethical approval was obtained for tissue analyses (REC reference 15/

NW/0429 and 19/NS/0167). Serial 5-μm sections were cut from each paraffin block and stained with hematoxylin and eosin (H&E) and immunoperoxidase immunohistochemistry (IHC). Tissue sections were assessed for cell density (H&E), microvessel surface area (CD31) and vascular permeability (fibrinogen) using immunoperoxidase IHC. Detailed protocols are described in Supporting Information Methods.

2.7 | Statistical analysis

Results from the computer simulation were used to quantitatively evaluate the LEGATOS method. The percentage deviation (PD) of the "measured" values from the "true" values were calculated, where PD = (measured − true)/true. Pixel-by-pixel calculation of PD within the 3D tumor region-of-interest for the patient was applied onto each of the 4 parametric maps derived using either the LEGATOS or the HTHS-merged method. Tumor mean and SD of the PD values were generated and compared between the 2 analysis approaches.
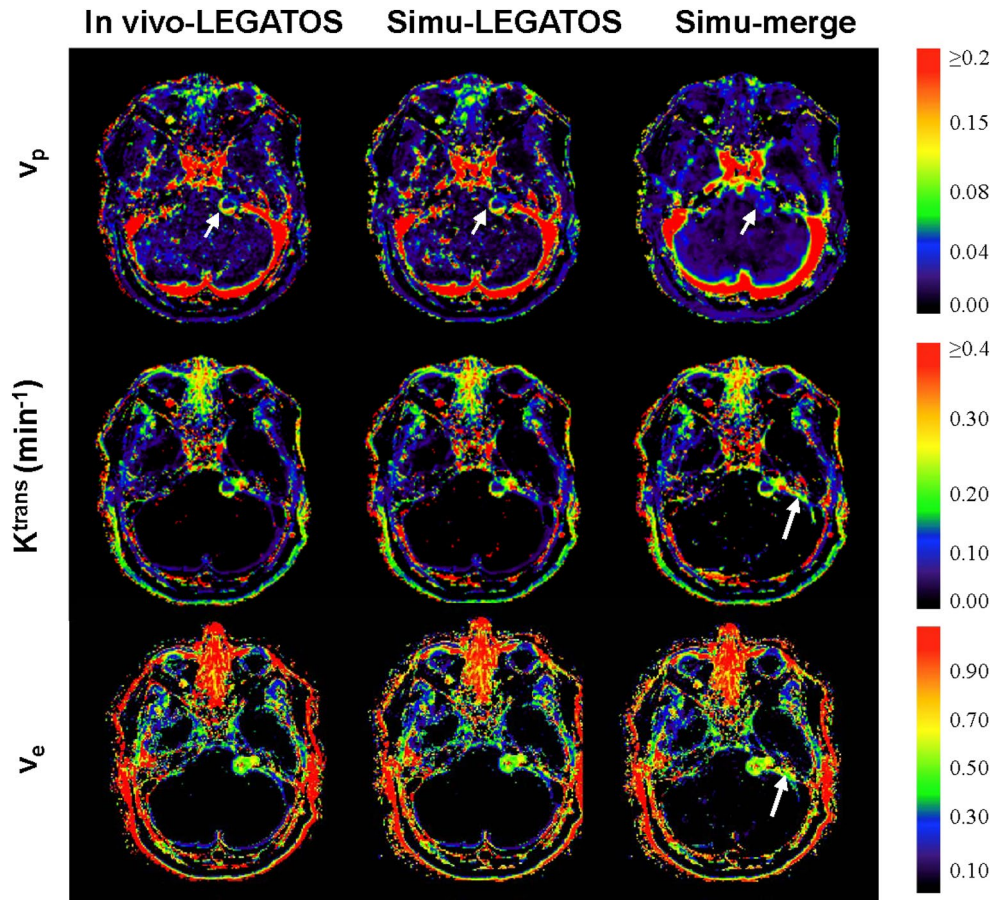
FIGURE 4 Comparison of kinetic parameter maps derived from computer-simulated dual injection DCE (DICE) data with the "true" in vivo parameter maps. The left-hand column (in vivo-LEGATOS) displays the LEGATOS-derived kinetic parameter maps (K^{trans}, v_p, and v_e) from the sporadic vestibular schwannoma (VS) patient DCE data displayed in Figure 3D, which were used as the "true" parameter values for DCE data simulation. The middle and right-hand column display the "measured" kinetic maps derived from analysis of the computer-simulated DICE data with either the LEGATOS (Simu-LEGATOS) or the HTHS-merged method (Simu-merge), respectively. Direct fitting of the simulated HTHS-merged data, without prior LEGATOS reconstruction produced a v_p map with comparatively less spatial detail (short arrow). K^{trans} and v_e maps derived directly from the simulated DICE data with the HTHS-merged method also demonstrated vessel contamination adjacent to the vestibular schwannoma on the left side (long arrow), an effect not seen in the LEGATOS derived images

For the in vivo study, mean tumor K^{trans} and v_p estimates derived from the 13 patients with GBM using either the LEGATOS approach or native LDHT data sets alone were compared using linear regression. For the 15 resected sporadic VS the inter-tumor correlation between DCE-MRI derived parameter estimates (K^{trans}, v_p, and v_e) and tissue-derived metrics (H&E cell density and CD31 microvessel surface area) are reported as Pearson's product moment correlation coefficient (r) or Spearman's ρ in the case of nonlinear associations.

3 | RESULTS

3.1 | Computer simulation

The combined low-dose VIF used for the in vivo LEGATOS analysis and the reconstructed full-dose VIF used for the FDHS 4D DCE volume simulations are shown in Figure 3A,B, respectively. A close similarity between the parenchymal tissue phase ($t > 40$ s) of the simulated low-dose GBCA concentration-time curves and the parenchymal phase of the simulated full-dose curves rescaled by the dose ratio was demonstrated (Figure 3C). This result supported the assumption that the LDHT and FDHS 4D concentration volumes can be merged through concatenation of the LDHT initial phase with later phases of the dose-calibrated FDHS 4D concentration volumes. A high similarity between the simulated and the in vivo acquired 4D FDHS DCE dynamic images was seen (Figure 3D) and the mean structural similarity index between the in vivo and the simulated 4D FDHS concentration volume was 0.998 ± 0.001 ($n = 35$ slices, range = 0.996-0.999).

Representative voxel fits of the in vivo acquired LDHT DCE-MRI data obtained from the patient imaged at 3T are shown in Supporting Information Figure S2 and demonstrate that when using the ETM, there is a good fit between the

scaled VIF and the early phase data of both tumor and normal appearing grey and white matter voxels. LEGATOS analysis of both the in vivo acquired and the computer simulated data produced highly comparable kinetic parameter maps (Figure 4). Tumoral vascular heterogeneity was clearly evident on the LEGATOS v_p maps derived using both the in vivo acquired and the computer simulated data but direct fitting of the simulated HTHS-merged data without prior LEGATOS reconstruction produced a v_p map with comparatively less spatial detail. The accuracy of kinetic parameter estimates was improved through use of the LEGATOS method compared to direct fitting of the simulated HTHS-merged data (v_p: mean PD $-1.4\% \pm 29.8\%$ vs. $13.9\% \pm 180\%$, $P = .05$; v_e: mean PD $0.8\% \pm 13.5\%$ vs. $11.7\% \pm 23.8\%$, $P < .001$; K^{trans}; mean PD $7.2\% \pm 12.3\%$ vs. $8.8\% \pm 78.4\%$, $P > .05$).

3.2 | In vivo evaluation

For the 17 patients with VS and 13 patients with GBM native tumor $R1_0$ estimates obtained from the VFA acquisitions before the LDHT DCE series are given in Table 1.

Comparative kinetic parameter maps from a patient with NF2 and bilateral VS imaged using the dual injection DTR protocol are shown in Figure 5A alongside fits of representative vessel voxel GBCA concentration-time curves obtained using each method. Compared to the use of native LDHT data sets the LEGATOS method offered superior visualization of small lesions and intratumoral heterogeneity in derived K^{trans} and v_p maps. The DICE-FDHS method also offered superior spatial resolution but because of undersampling of the first-pass bolus in each pixel-enhancing curve, derived K^{trans} and v_p maps suffered from large vessel contamination and lack of vessel contrast, respectively, features not seen in the LDHT- or LEGATOS-derived maps. As shown in Figure 5B, whereas the DICE-FDHS method demonstrates poor discrimination between plasma volume and vascular leakage effects giving a very high value of K^{trans} (=1.1 min^{-1}) and low value of v_p (=0.04) within the vessel, voxel fits of the native LDHT, HTHS-merged, and LEGATOS concentration-time curves produced lower K^{trans} and higher v_p values, respectively.

Representative tumor maps of K^{trans} and v_p in 2 patients with glioblastoma are shown in Figure 6 and Supporting

Information Figure S3. Similar to the findings in VS, LEGATOS permitted superior visualization of microvascular heterogeneity in the contrast enhancing tumor edge compared to maps derived from the LDHT data sets alone. Estimates of mean tumor K^{trans} and v_p derived from the contrast enhancing tumor region of the 13 imaged glioblastoma are shown in Figure 6C and demonstrate the strong correlation between K^{trans} ($R^2 = 0.88$, $P < .0001$) and v_p estimates ($R^2 = 0.79$, $P < .0001$) derived using either the LEGATOS approach or native LDHT data sets alone.

3.3 | Imaging and pathology analysis

The inter-tumor correlation between LEGATOS derived kinetic parameter estimates and tissue metrics in the 15 sporadic VS that underwent the dual injection DTR protocol are shown in Figure 7. There was a significant inverse correlation between cell density and mean tumor v_e ($\rho = -0.69$, $P = .006$, Figure 7A) and a significant positive correlation between CD31 % microvessel surface area with both mean tumor v_p ($r = 0.85$, $P = .001$, Figure 7B) and mean tumor K^{trans} ($r = 0.71$, $P = .003$, Figure 7C).

Representative imaging and tissue from a patient with a sporadic VS imaged at 1.5T is shown in Figure 8. Compared to use of the native LDHT data sets, the LEGATOS reconstruction method permitted better characterization of spatial heterogeneity in cell density and microvascular metrics across the tumor volume.

4 | DISCUSSION

We have described LEGATOS: a novel DTR DCE-MRI processing approach for deriving accurate, HS resolution, and whole-brain coverage kinetic parameter maps. Data from computer simulations and in vivo imaging demonstrated that kinetic parameters derived using LEGATOS provided superior discrimination of plasma volume and vascular leakage effects compared to other HS resolution approaches. Comparison with matched tumor tissue demonstrated that LEGATOS derived microvascular parameters accurately differentiated inter-tumor differences in microvessel surface

Tumor	n	Field strength (T)	Native $R1_0$ before LDHT DCE series (s^{-1})
Sporadic VS	15	1.5	0.68 ± 0.03
Sporadic VS	1	3	0.48
NF2-related VS	1	1.5	0.62
GBM	13	1.5	0.74 ± 0.12

TABLE 1 Tumor mean native $R1_0$ estimated from the VFA acquisitions for the 17 patients with VS and 13 patients with GBM

Abbreviations: GBM, glioblastoma; VS, vestibular schwannoma.
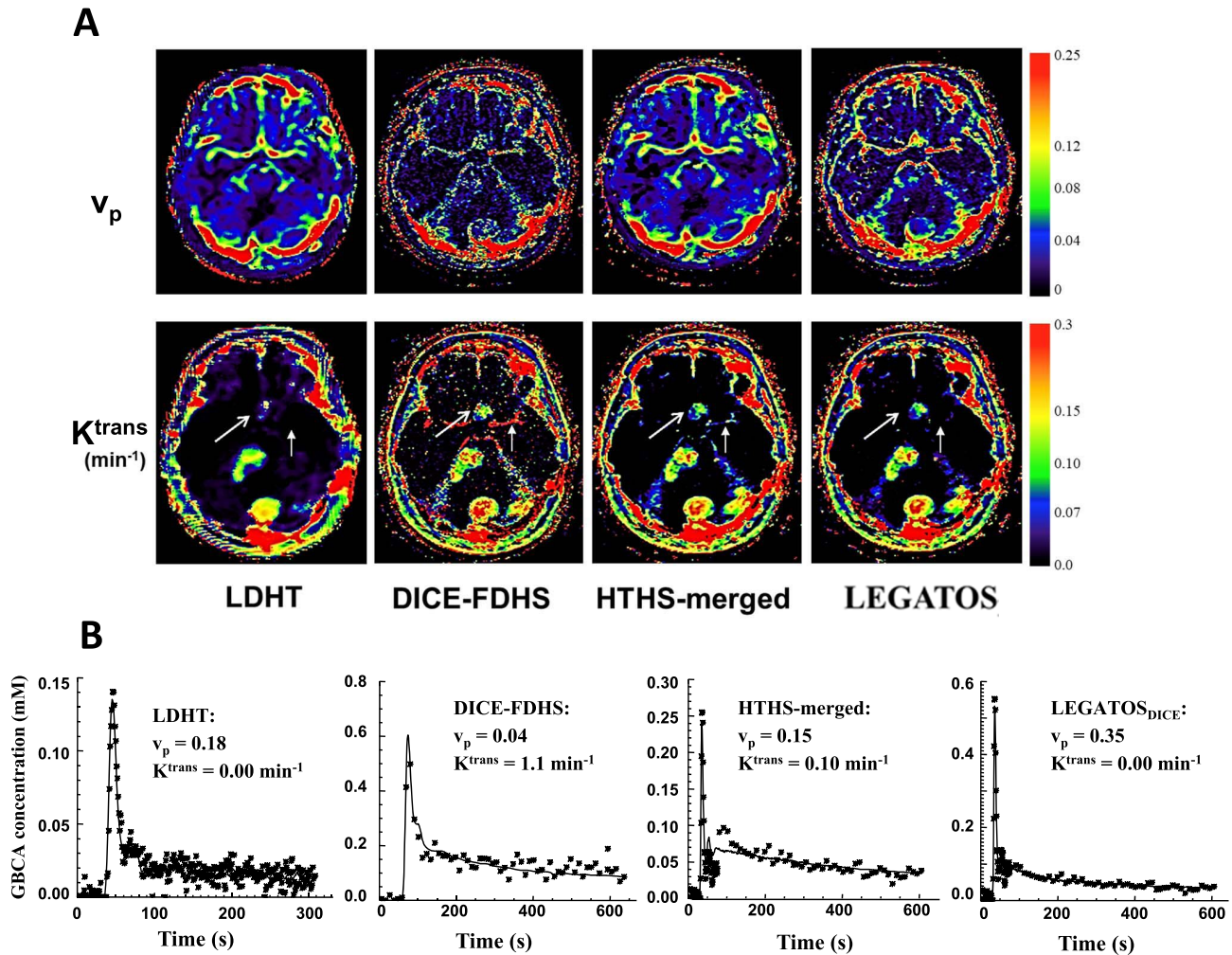
A

B

FIGURE 5 Kinetic parameter maps from a neurofibromatosis type-2 patient imaged using a dual injection, dual-temporal resolution protocol. (A) K^{trans} and v_p maps obtained from dual injection DCE (DICE) MRI at 1.5T are shown. Note the large right-sided VS and multiple supra- and infra-tentorial meningiomas in this patient. Maps derived using the native low-dose high-temporal resolution tissue concentration-time curves (LDHT), the native full-dose high-spatial resolution tissue concentration-time curves (DICE-FDHS method), the HTHS-merged data and the LEGATOS reconstructed data are shown. Although the LDHT derived K^{trans} map appears free of large vessel contamination, the small tuberculum sellae meningioma (long arrow) is difficult to visualize. The DICE-FDHS derived maps better demonstrate this meningioma and intratumoral heterogeneity within the VS but show considerable large vessel contamination (short arrow). The degree of large vessel contamination is reduced in the HTHS-merged data and almost absent in the LEGATOS derived K^{trans} map. Relative to the HTHS-merged data, the LEGATOS map displayed greater spatial detail in the derived v_p map. (B) Fits of representative vessel voxel GBCA concentration-time curves with the ETM. Fits obtained using each method shown. The DICE-FDHS method demonstrate poor discrimination of plasma volume and vascular leakage effects in the vessel GBCA concentration-time curve giving a high value of K^{trans} (=1.1 min^{-1}) and low value of v_p (=0.04) within the vessel. Voxel fits of the native LDHT, HTHS-merged, and LEGATOS concentration-time curves produced lower K^{trans} and higher v_p values, respectively

area and cell density and permitted better evaluation of intratumoral heterogeneity in these tissue metrics compared to HT data alone.

Previous attempts to derive HS kinetic parameters from DTR DCE-MRI such as the DICE-FDHS method[17] showed significant covariate fitting errors in derived parameter maps because of the low-temporal resolution of the sampled tissue uptake curves. Our strategy overcomes this limitation by first merging the separately acquired HT (low-spatial) and HS (low-temporal) DCE-MRI data sets into a merged 4D GBCA concentration-time course, and second rescaling

the HT arterial phase of this HTHS-merged concentration-time course to match the "true" HS one, before subsequent kinetic analysis. We hypothesized that HT sampling of the initial part of the tissue uptake curves would address fitting errors induced by temporal jitter uncertainty (uncertainty in time alignment of the arterial input function and tissue uptake curves)[29] and undersampling at the bolus peak. Our acquired data supported this with the LEGATOS derived parameter maps demonstrating superior separation of plasma volume and vascular leakage-based changes in the tissue GBCA concentration-time course.
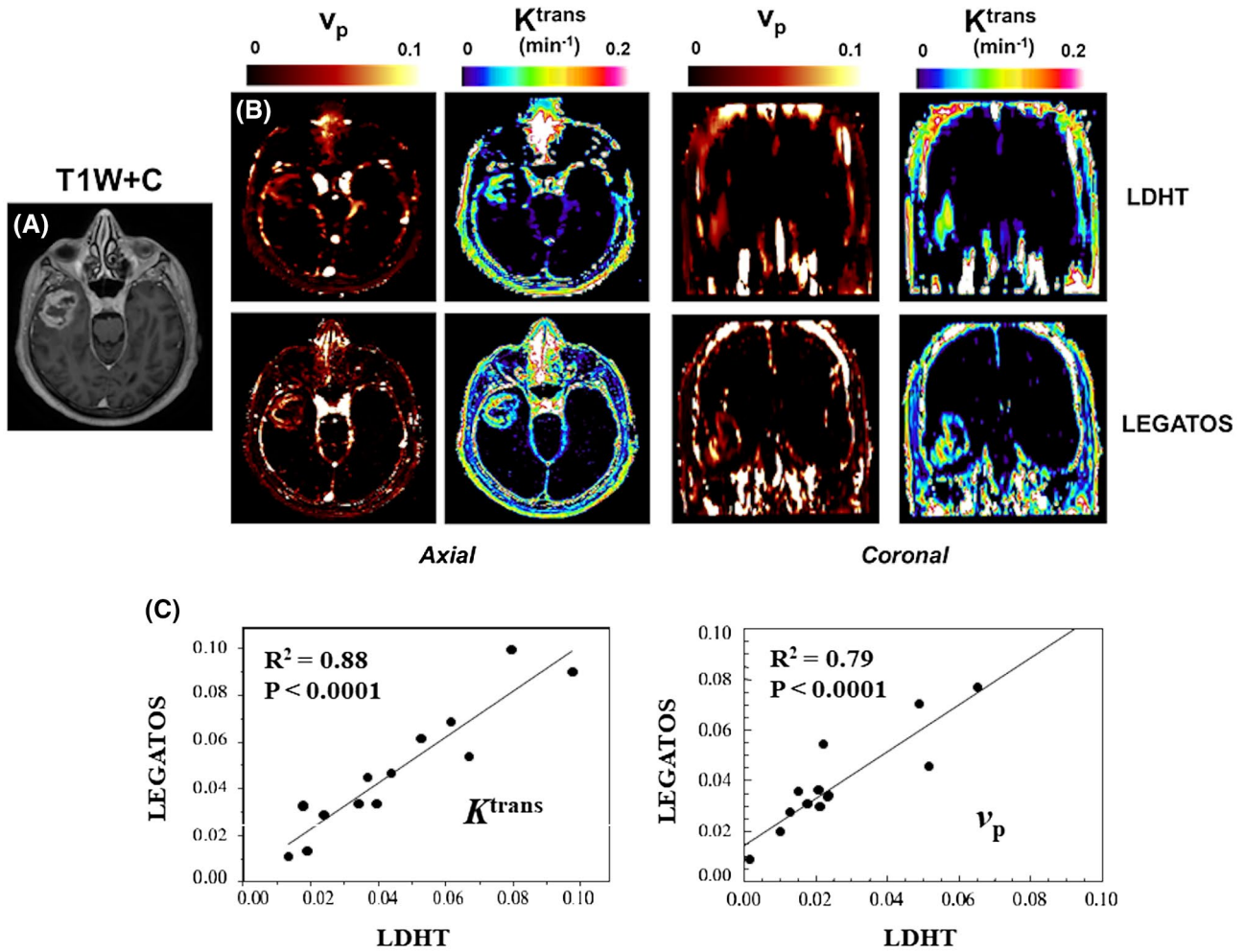
FIGURE 6 Application of the LEGATOS technique in a patient with a right temporal glioblastoma (GBM). (A) T1W post contrast image demonstrating a right temporal glioblastoma (GBM). Note the contrast enhancing tumor rim and the non-enhancing central necrotic core. (B) Kinetic parameter maps of the GBM shown in panel A. From left to right: parametric v_p and K^{trans} map in axial plane; and parametric v_p and K^{trans} map in coronal plane. Note the superior visualization of normal vascular anatomy and microvascular heterogeneity in the contrast enhancing tumor edge permitted by the LEGATOS technique compared to maps derived from the native low-dose high-temporal (LDHT) data sets. (C) Mean tumor K^{trans} (left) and v_p (right) estimates derived from the contrast enhancing tumor region of the 13 imaged GBM using the LDHT and LEGATOS methods. The left panel demonstrates the strong correlation between K^{trans} estimates derived using the LEGATOS approach and estimates derived from the native LDHT data sets alone ($R^2 = 0.88$, $P < .0001$). The right panel demonstrates the strong correlation between v_p estimates derived using the LEGATOS approach and estimates derived from the native LDHT data sets alone ($R^2 = 0.79$, $P < .0001$)

Previous in vivo studies in sporadic VS have demonstrated that kinetic parameter estimates derived through use of the ETM with low-spatial, HT resolution DCE-MRI accurately reflect inter-tumor differences in tissue vascularity metrics and correlate with differences in macrophage content and tumor growth rate.[5,30] However, the inherent low-spatial resolution in derived parameter maps limited accurate assessment of intratumoral heterogeneity, especially within smaller lesions. In the present study we demonstrated that HS resolution LEGATOS derived microvascular parameters permitted better evaluation of intratumoral heterogeneity in microvessel area and cell density compared to HT data alone and accurately differentiated inter-tumor differences in these tissue parameters. The LEGATOS-derived mean tumor v_e showed

an inverse correlation with cell density, and both the mean tumor v_p and mean tumor K^{trans} showed a positive correlation with CD31 % microvessel surface area. Although a limitation of any non-invasive imaging technique such as DCE-MRI is that the true in vivo tissue perfusion parameters are unknown and can only be extrapolated from architectural features detectable on ex vivo tissue specimens such as microvessel density and microvessel surface area, the correlation between CD31 and both DCE-MRI derived v_p and K^{trans} has been previously reported in human vessel wall studies.[31-33]

Previous authors have attempted to achieve high spatiotemporal resolution in DCE-MRI through the use of advanced time resolved or "keyhole" imaging techniques[34] such as Siemens TWIST,[35] Phillips 4D-TRAK,[36] GE's
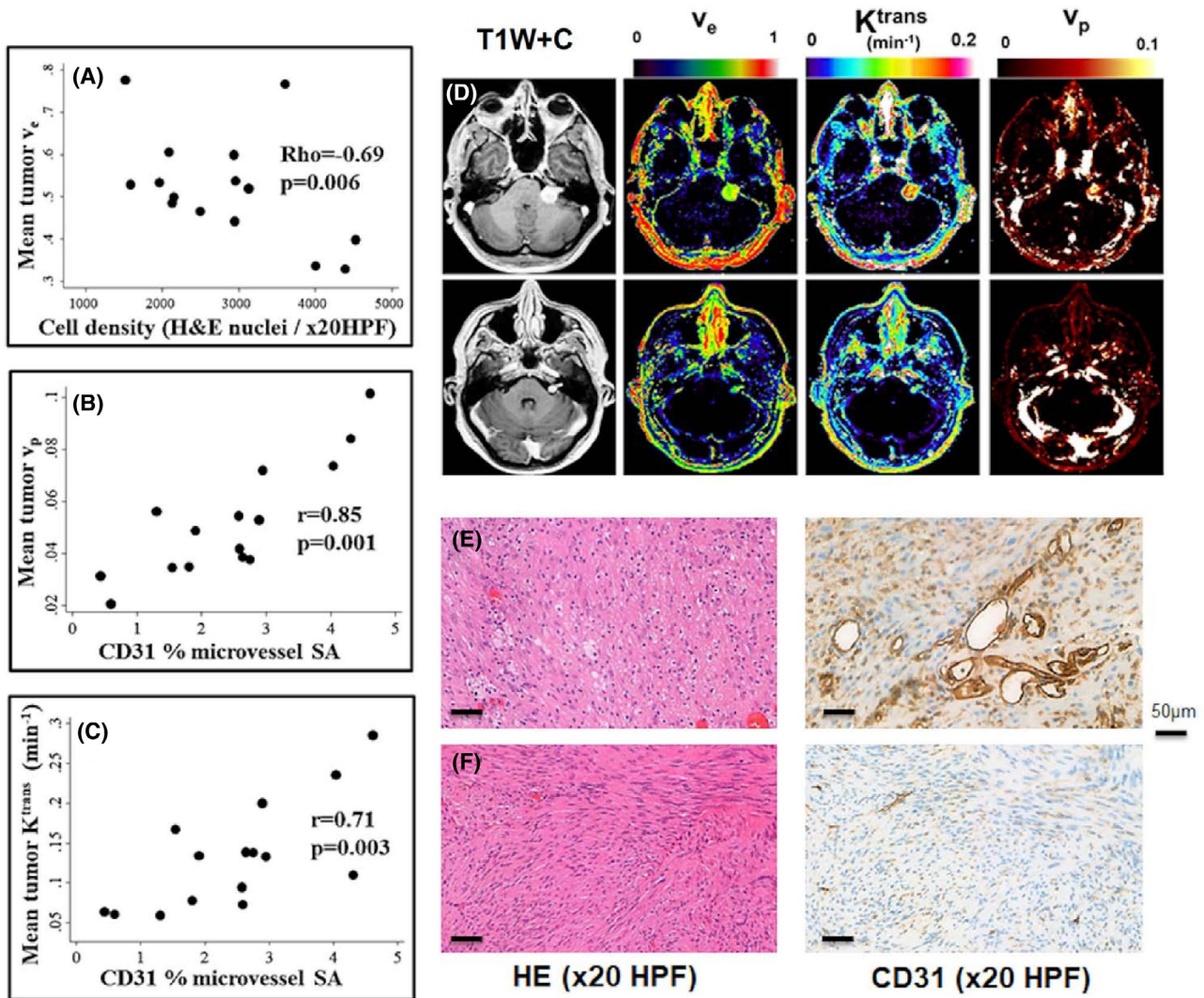
FIGURE 7 Comparison of LEGATOS derived parameters from the dual injection DTR DCE-MRI data sets against tissue derived parameters. (A) Inter-tumor scatterplot comparison of mean tumor v_e estimates against hematoxylin and eosin (H&E) cell density (nuclei/ x20HPF). (B) Inter-tumor scatterplot analysis of mean vascular fraction (v_p) against mean CD31 % microvessel surface area (SA). (C) Inter-tumor scatterplot analysis of mean tumor K^{trans} (min^{-1}) against mean CD31 % microvessel surface area (SA). (D) Representative LEGATOS derived kinetic parameter maps from a patient with a growing highly vascular VS (top row) and a less vascular static VS (bottom row) are shown. From left to right: T_1W post contrast image; parametric v_e map; parametric K^{trans} map, and parametric v_p map. (E-F) H&E stained section (left, HE-x20HPF) and immunostain (right, CD31, brown; immunoperoxidase –x20HPF) from the growing (top row) and static (bottom row) VS shown in panel D. Note the lower cell density (HE) and higher microvessel density (CD31) in the growing VS in keeping with the imaging findings. Data from 15 tumors (sporadic VS) shown. **Pearson's product moment correlation coefficient (r) reported or Spearman's ρ in the case of non-linear association between variables

TRICKS,[37] and DISCO.[38] Such techniques improved temporal resolution during data acquisition through undersampling of peripheral k-space. There has also been growing interest in estimating kinetic parameters directly from undersampled k-,t-space data without prior data reconstruction.[39,40] Our dual injection DTR DCE-MRI approach, however, offers greater temporal resolution during image acquisition ($\Delta t < 1.5$ s) compared to many of the above techniques, and a distinct advantage of the presented LEGATOS method is that it can be retrospectively acquired to dual injection DTR DCE-MRI data without the need for peripheral k-space undersampling.

In addition to its demonstrated application with full-dose DTR protocols, applicability of LEGATOS with a single injection low GBCA dose (fixed volume of 3 mL) interleaved HT and HS protocol has also been demonstrated in preliminary prospective unpublished studies at our institution.[21] Although the risk of gadolinium deposition in the brain following administration of macrocyclic GBCA such as gadoterate meglumine is thought to be lower than linear agents and the long-term clinical sequelae of such deposition is currently unknown[12,13] the ability to derive HS resolution kinetic parameter data following a low-dose administration may still have considerable clinical relevance, especially in patients
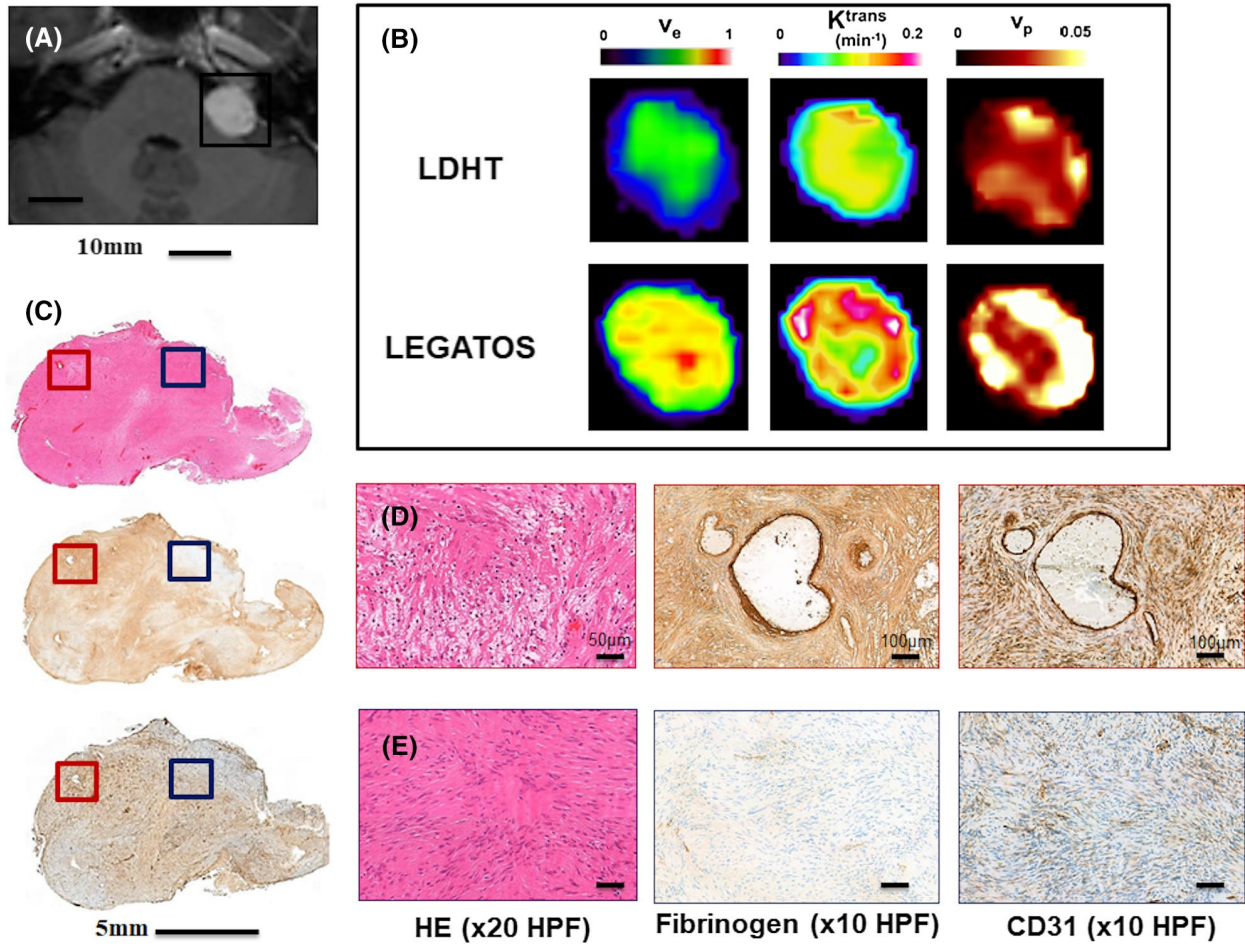
FIGURE 8 Evaluation of heterogeneity in tumor microvascular metrics using the LEGATOS technique. (A) T_1W post contrast image demonstrating growing left sided VS, note the heterogenous enhancement within the tumor. Scale bar = 10 mm. (B) Kinetic parameter maps (v_e, K^{trans}, and v_p) of the VS shown in panel A derived using dual injection DTR DCE-MRI. Parameter maps derived from the native LDHT data sets (top row, LDHT) and the LEGATOS reconstructed data sets (bottom row, LEGATOS) are shown. Note the spatial heterogeneity in LEGATOS derived v_e, K^{trans}, and v_p values across the imaged tumor slice. (C) Hematoxylin and eosin (H&E) stained section (top, HE-whole mount) and immunostains (middle, fibrinogen, brown; bottom, CD31, brown; immunoperoxidase—whole mount) from the tumor shown in panel A/B demonstrate heterogeneity in cell density (H&E), perivascular leak (fibrinogen) and microvessel density (CD31) across the tumor section. (D and E) Higher magnification images of the areas framed in the whole mount demonstrating regions of high (D) and low (E) cell density (HE, ×20 HPF), perivascular leak (fibrinogen, immunoperoxidase ×10 HPF) and microvessel density (CD31, immunoperoxidase × 10 HPF)

undergoing repeated GBCA exposures and in clinical trials where microvascular parameters are felt to be relevant outcome markers such as trials of antiangiogenic treatment.[41] Further studies incorporating the LEGATOS technique and low GBCA dose acquisition protocols are, however, required to better evaluate the effect of this low-dose approach on image contrast-to-noise, and the accuracy of kinetic parameters derived using this technique.[21]

The proposed LEGATOS method relies on the assumption that in each pixel of the HTHS-merged 4D concentration volume generated in key step I, the supposed "true" HS resolution arterial phase has the same shape as the observed $HT_{aligned}$ arterial phase, and therefore, can be obtained by rescaling the $HT_{aligned}$ arterial phase to achieve a smooth connection with the HS parenchymal phase. The ETM further

assumes that the arterial phase of each enhanced tissue pixel curve is the initial plasma concentration curve scaled by v_p. However, the above assumption may not be met if the $HT_{aligned}$ and "true" HS concentration curves display significant differences in the bolus mean transit time and/or in the amount of GBCA leakage. In this case, reconstruction of the initial HT contrast agent concentration curve using a single concentration ratio is not suitable and more complex adjustment may be required.

The ETM has been adopted in this study as previous application of this model with low-spatial resolution HT data sets derived from DTR DCE-MRI was found to give both tissue-validated and clinically relevant kinetic parameter estimates.[4,5,30] Recent studies have also shown through a model selection process using the Akaike information

criteria, that the ETM was one of the optimal models in pharmacokinetic analysis of DCE-MRI data in brain tumors[42] and papillary thyroid carcinoma.[43] One limitation of the ETM is that the derived parameter K^{trans} is a hybrid parameter reflecting both capillary blood flow and permeability effects,[44,45] and future studies incorporating the high spatiotemporal resolution DCE data provided by the LEGATOS method and other DCE-MRI models, which seek to further separate out such effects should, therefore, be undertaken.

5 | CONCLUSION

We developed a novel DTR technique called LEGATOS to generate HS resolution kinetic parametric maps with an accuracy normally only obtainable with HT ($\Delta t < 1.5$ s), low-spatial resolution DCE-MRI. The accuracy of kinetic parameters estimated using this new technique outperformed previous DTR methods for deriving HS resolution parameter maps and analysis of tissue from VS investigated with LEGATOS validated our approach. Clinical application of this modality and its application with low GBCA dose DCE-MRI protocols require further studies.

ORCID
Ka-Loh Li https://orcid.org/0000-0002-6051-9248

REFERENCES
1. O'Connor JP, Jackson A, Parker GJ, Roberts C, Jayson GC. Dynamic contrast-enhanced MRI in clinical trials of antivascular therapies. *Nat Rev Clin Oncol*. 2012;9:167-177.
2. Essig M, Anzalone N, Combs SE, et al. MR imaging of neoplastic central nervous system lesions: review and recommendations for current practice. *AJNR Am J Neuroradiol*. 2012;33:803-817.
3. Jain R. Measurements of tumor vascular leakiness using DCE in brain tumors: clinical applications. *NMR Biomed*. 2013;26:1042-1049.
4. Li KL, Djoukhadar I, Zhu X, et al. Vascular biomarkers derived from dynamic contrast-enhanced MRI predict response of vestibular schwannoma to antiangiogenic therapy in type 2 neurofibromatosis. *Neuro Oncol*. 2016;18:275-282.
5. Lewis D, Roncaroli F, Agushi E, et al. Inflammation and vascular permeability correlate with growth in sporadic vestibular schwannoma. *Neuro Oncol*. 2019;21:314-325.
6. Larsson HB, Courivaud F, Rostrup E, Hansen AE. Measurement of brain perfusion, blood volume, and blood-brain barrier permeability, using dynamic contrast-enhanced T(1)-weighted MRI at 3 Tesla. *Magn Reson Med*. 2009;62:1270-1281.
7. van Dijken BRJ, van Laar PJ, Smits M, Dankbaar JW, Enting RH, van der Hoorn A. Perfusion MRI in treatment evaluation of glioblastomas: clinical relevance of current and future techniques. *J Magn Reson Imaging*. 2019;49:11-22.
8. Jackson A, O'Connor JP, Parker GJ, Jayson GC. Imaging tumor vascular heterogeneity and angiogenesis using dynamic contrast-enhanced magnetic resonance imaging. *Clin Cancer Res*. 2007;13:3449-3459.
9. O'Connor JP, Jackson A, Parker GJ, Jayson GC. DCE-MRI biomarkers in the clinical evaluation of antiangiogenic and vascular disrupting agents. *Br J Cancer*. 2007;96:189-195.
10. Ingrisch M, Sourbron S, Morhard D, et al. Quantification of perfusion and permeability in multiple sclerosis: dynamic contrast-enhanced MRI in 3D at 3T. *Invest Radiol*. 2012;47:252-258.
11. Rose CJ, O'Connor JP, Cootes TF, et al. Indexed distribution analysis for improved significance testing of spatially heterogeneous parameter maps: application to dynamic contrast-enhanced MRI biomarkers. *Magn Reson Med*. 2014;71:1299-1311.
12. Mallio CA, Rovira À, Parizel PM, Quattrocchi CC. Exposure to gadolinium and neurotoxicity: current status of preclinical and clinical studies. *Neuroradiology*. 2020;62:925-934.
13. Gulani V, Calamante F, Shellock FG, Kanal E, Reeder SB. Gadolinium deposition in the brain: summary of evidence and recommendations. *Lancet Neurology*. 2017;16:564-570.
14. Cramer SP, Simonsen H, Frederiksen JL, Rostrup E, Larsson HB. Abnormal blood-brain barrier permeability in normal appearing white matter in multiple sclerosis investigated by MRI. *Neuroimage Clin*. 2014;4:182-189.
15. Kershaw LE, Buckley DL. Precision in measurements of perfusion and microvascular permeability with T1-weighted dynamic contrast-enhanced MRI. *Magn Reson Med*. 2006;56:986-992.
16. Barnes SR, Ng TS, Montagne A, Law M, Zlokovic BV, Jacobs RE. Optimal acquisition and modeling parameters for accurate assessment of low Ktrans blood-brain barrier permeability using dynamic contrast-enhanced MRI. *Magn Reson Med*. 2015;75:1967-1977.
17. Li KL, Buonaccorsi G, Thompson G, et al. An improved coverage and spatial resolution–using dual injection dynamic contrast-enhanced (ICE-DICE) MRI: a novel dynamic contrast-enhanced technique for cerebral tumors. *Magn Reson Med*. 2012;68:452-462.
18. Kostler H, Ritter C, Lipp M, Beer M, Hahn D, Sandstede J. Prebolus quantitative MR heart perfusion imaging. *Magn Reson Med*. 2004;52:296-299.
19. Li K-L, Lewis D, Jackson A, Zhao S, Zhu X. Improving quantification accuracy in whole brain high spatial resolution 3D kinetic mapping: Development of a novel dual temporal resolution DCE-MRI technique. In Proceedings of the 27th Annual Meeting of ISMRM, Montreal, Canada, 2019. p. 4409. 2019.
20. Li K-L, Lewis D, Zhao S, Jackson A, Zhu X. Accuracy assessment of high-spatial resolution whole-brain tracer-kinetic parameter maps generated using dual-temporal resolution DCE-MRI.

In Proceedings of the 28th Annual Meeting of ISMRM, 2020. p. 3779. 2020.

21. Li K-L, Lewis D, Coope DJ, et al. Feasibility of a single low dose dual temporal resolution DCE-MRI method for whole-brain, high-spatial resolution parametric mapping. In Proceedings of the 29th Annual Meeting of ISMRM, 2021. p. 0915. 2021.

22. Ashburner J, Friston K. Multimodal image coregistration and partitioning—a unified framework. *Neuroimage*. 1997;6:209-217.

23. Tofts PS. Modeling tracer kinetics in dynamic Gd-DTPA MR imaging. *J Magn Reson Imaging*. 1997;7:91-101.

24. Fritz-Hansen T, Rostrup E, Sondergaard L, Ring PB, Amtorp O, Larsson HB. Capillary transfer constant of Gd-DTPA in the myocardium at rest and during vasodilation assessed by MRI. *Magn Reson Med*. 1998;40:922-929.

25. Gowland P, Mansfield P, Bullock P, Stehling M, Worthington B, Firth J. Dynamic studies of gadolinium uptake in brain tumors using inversion- recovery echo-planar imaging. *Magn Reson Med*. 1992;26:241-258.

26. Li KL, Zhu X, Zhao S, Jackson A. Blood-brain barrier permeability of normal-appearing white matter in patients with vestibular Schwannoma: a new hybrid approach for analysis of T1 -W DCE-MRI. *J Magn Reson Imaging*. 2017;46:79-93.

27. Li KL, Wilmes LJ, Henry RG, et al. Heterogeneity in the angiogenic response of a BT474 human breast cancer to a novel vascular endothelial growth factor-receptor tyrosine kinase inhibitor: assessment by voxel analysis of dynamic contrast-enhanced MRI. *J Magn Reson Imaging*. 2005;22:511-519.

28. Wang Z, Bovik AC, Sheikh HR, Simoncelli EP. Image quality assessment: from error visibility to structural similarity. *IEEE Trans Image Process*. 2004;13:600-612.

29. Henderson E, Rutt BK, Lee TY. Temporal sampling requirements for the tracer kinetics modeling of breast disease. *Magn Reson Imaging*. 1998;16:1057-1073.

30. Lewis D, Donofrio CA, O'Leary C, et al. The microenvironment in sporadic and neurofibromatosis type II-related vestibular schwannoma: the same tumor or different? A comparative imaging and neuropathology study. *J Neurosurg*. 2021;134:1419-1429.

31. Kerwin W, Hooker A, Spilker M, et al. Quantitative magnetic resonance imaging analysis of neovasculature volume in carotid atherosclerotic plaque. *Circulation*. 2003;107:851-856.

32. Taqueti VR, Di Carli MF, Jerosch-Herold M, et al. Increased microvascularization and vessel permeability associate with active inflammation in human atheromata. *Circ Cardiovasc Imaging*. 2014;7:920-929.

33. Coolen BF, Calcagno C, van Ooij P, Fayad ZA, Strijkers GJ, Nederveen AJ. Vessel wall characterization using quantitative MRI: what's in a number? *Magn Reson Mater Phy*. 2018;31:201-222.

34. van Vaals JJ, Brummer ME, Dixon WT, et al. "Keyhole" method for accelerating imaging of contrast agent uptake. *J Magn Reson Imaging*. 1993;3:671-675.

35. Song T, Laine AF, Chen Q, et al. Optimal k-space sampling for dynamic contrast-enhanced MRI with an application to MR renography. *Magn Reson Med*. 2009;61:1242-1248.

36. Shin SU, Cho N, Kim SY, Lee SH, Chang JM, Moon WK. Time-to-enhancement at ultrafast breast DCE-MRI: potential imaging biomarker of tumour aggressiveness. *Eur Radiol*. 2020;30:4058-4068.

37. Korosec FR, Frayne R, Grist TM, Mistretta CA. Time-resolved contrast-enhanced 3D MR angiography. *Magn Reson Med*. 1996;36:345-351.

38. Saranathan M, Rettmann DW, Hargreaves BA, Clarke SE, Vasanawala SS. DIfferential Subsampling with Cartesian Ordering (DISCO): a high spatio-temporal resolution Dixon imaging sequence for multiphasic contrast enhanced abdominal imaging. *J Magn Reson Imaging*. 2012;35:1484-1492.

39. Guo Y, Lingala SG, Zhu Y, Lebel RM, Nayak KS. Direct estimation of tracer-kinetic parameter maps from highly undersampled brain dynamic contrast enhanced MRI. *Magn Reson Med*. 2017;78:1566-1578.

40. Guo Y, Lingala SG, Bliesener Y, Lebel RM, Zhu Y, Nayak KS. Joint arterial input function and tracer kinetic parameter estimation from undersampled dynamic contrast-enhanced MRI using a model consistency constraint. *Magn Reson Med*. 2018;79:2804-2815.

41. Gong E, Pauly JM, Wintermark M, Zaharchuk G. Deep learning enables reduced gadolinium dose for contrast-enhanced brain MRI. *J Magn Reson Imaging*. 2018;48:330-340.

42. Inglese M, Ordidge KL, Honeyfield L, et al. Reliability of dynamic contrast-enhanced magnetic resonance imaging data in primary brain tumours: a comparison of Tofts and shutter speed models. *Neuroradiology*. 2019;61:1375-1386.

43. Paudyal R, Lu Y, Hatzoglou V, et al. Dynamic contrast-enhanced MRI model selection for predicting tumor aggressiveness in papillary thyroid cancers. *NMR Biomed*. 2020;33:e4166.

44. Tofts PS, Brix G, Buckley DL, et al. Estimating kinetic parameters from dynamic contrast-enhanced T(1)-weighted MRI of a diffusable tracer: standardized quantities and symbols. *J Magn Reson Imaging*. 1999;10:223-232.

45. Sourbron SP, Buckley DL. On the scope and interpretation of the Tofts models for DCE-MRI. *Magn Reson Med*. 2011;66:735-745.

SUPPORTING INFORMATION

Additional Supporting Information may be found online in the Supporting Information section.

FIGURE S1 Vascular input function (VIF) estimation from the middle cerebral artery (MCA), the internal carotid artery (ICA), and the superior sagittal sinus (SSS). Plasma GBCA concentration curves $C_p(t)$ measured from the horizontal segment of the MCA; the vertical segment of the internal carotid artery (ICA; ie, carotid syphon); and the vertical segment of the (SSS) following a bolus injection of 0.02 mmol/kg of macrocyclic GBCA (gadoterate meglumine; Dotarem, Guerbet S.A). The first-pass data are fitted using a γ variate function, which excludes GBCA bolus recirculation. The first-pass bolus kinetic parameters from each derived VIF, including the contrast bolus arrival time (BAT), the full width at half maximum (FWHM) and peak height (peak), are shown. Although the BAT in the SSS is 3.4 s later than the ICA, the VIF measured from the SSS has a higher and narrower peak than those measured from the corresponding arterial vessels. Reduced partial volume effects when performing VIF measurement within the wider SSS, and may in part explain the higher and narrower peak observed. In addition, reduced "in flow" effects because of both lower blood velocity in the SSS and a longer transit time within

the imaging volume for measured blood within the SSS (and thereby more received RF pulses) compared to blood within the ICA or MCA, which may also contribute to the observed differences. All images and VIF estimates obtained from a patient with a sporadic VS imaged at 1.5T. GBCA = gadolinium-based-contrast agent

FIGURE S2 GBCA concentration—(A) time curves from representative voxels within tumor tissue; (B) normal-appearing grey matter (GM); and (C) normal appearing white matter (WM). Voxel curves derived from low-dose high-temporal (LDHT) DCE-MRI data in a sporadic VS patient imaged at 3T. Fits obtained using the extended Tofts model (ETM) for each voxel curve are shown on the included figures (solid line) along with the derived parameter estimates. Normal-appearing GM or WM have a K^{trans} too low to be measured using the ETM, giving zero K^{trans} for both the GM and WM voxels. The above curves demonstrate that when using the ETM, there is a good fit between the scaled VIF and the early phase data of tumor, or normal-appearing GM or WM voxels and that the degree of dispersion in the tissue or widening of the concentration-time curve in each tissue voxel

during the first pass is consistent within each patient. GBCA = gadolinium-based-contrast agent

FIGURE S3 Application of the LEGATOS technique in a patient with left parietal glioblastoma (GBM). (A) T_1W post contrast image demonstrating a left parietal glioblastoma (GBM). (B) Kinetic parameter maps of the GBM shown in panel A. From left to right: parametric K^{trans} map, parametric v_p map and magnification images demonstrating voxel-wise heterogeneity in K^{trans} and v_p across the tumor. Parameter maps derived from the native low-dose high-temporal resolution data sets (top row, LDHT) and the LEGATOS reconstructed data sets (bottom row, LEGATOS) are shown